Applied Catalysis B: Environment and Energy 356 (2024) 124252

Contents lists available at ScienceDirect

Applied Catalysis B: Environment and Energy

journal homepage: www.elsevier.com/locate/apcatb

In situ redox growth of Pd/CuO_x for enhanced electrocatalytic degradation of organic chlorides via indirect atomic H* reduction

Yun Guo, Yang Li, Wei Shi, Jia Yuan, Li Wang *, Zhiwei Wang *

State Key Laboratory of Pollution Control and Resource Reuse, Shanghai Institute of Pollution Control and Ecological Security, Tongji Advanced Membrane Technology Center, School of Environmental Science and Engineering, Tongji University, 1239 Siping Road, Shanghai 200092, China

ARTICLE INFO

Keywords:
Organic chlorides
Copper oxides
Atomic hydrogen
Electrocatalytic dechlorination
2
4-D

ABSTRACT

Efficient utilization of atomic hydrogen (H*) is crucial for electrocatalytic dechlorination. We synthesized a Pd/CuO_x cathode by atomic reconstruction to boost H* utilization, creating additional active sites within a biphasic interface. This enhanced H* generation degraded 2,4-dichlorophenoxyacetic acid (2,4-D) with a 96 % removal efficiency at 4 mA cm^{-2} and 1.96 kWh m^{-3} energy consumption. Cyclic voltammetry (CV) showed a 0.009 μmol cm^{-2} increase H* on the Pd/CuO_x cathode compared to the pristine Cu cathode. The contribution of H* to the electrocatalytic dechlorination process was further corroborated by scavenging experiments and electron spin resonance investigation. We then evaluated the toxicity of products during the degradation process. Density functional theory calculations revealed that the coordination structure between CuO_x and Pd optimized the dissociation of H_2O and the free adsorption energy of hydrogen. This research introduces an effective alternative to enhance the H* production for the removal of organochlorine compounds from wastewater.

1. Introduction

Organic chlorides (OCs) are a group of organic compounds that hydrogen atoms are replaced by chlorine atoms, and are widely used in industry, agriculture and chemical engineering [1–3]. OCs are frequently detected in the environment and animal bodies due to bioaccumulation and biomagnification [4–6]. Because they are highly cytotoxic, carcinogenic and bioaccumulative, OCs are listed as persistent organic pollutants (POPs), and classified as priority pollutants by the US Environmental Protection Agency [1,7–9].

Electrochemical reduction is a promising method for breaking highly stable carbon–chloride bonds (340 kJ mol^{-1}) by direct reduction, involving direct reaction with atomic H* (—2.1 V vs RHE) and/or cathodic reduction by transferring electrons [10–12]. However, at the cathode surface, hydrogen evolution reaction (HER) is a primary process and therefore hinders atomic H* participating electrochemical dechlorination. In this regard, noble metal catalysts (e.g., Pt [13], Pd [14,15], Ru [16] and Au [17]) and their alloys [18–21]) have been explored as they can generate a large amount of atomic H* by water reduction. Nevertheless, the high price of such noble metals and the environmental impacts of metal mining significantly limit their widespread applications [13].

Lately, Cu-based materials have attracted considerable attention as alternatives for electrochemical reduction. Based on the Nørskov volcano theory, Cu with full d electrons of $3d^{10}4s^1$ has a weak binding capacity for H* [22], decreasing the HER efficiency. At the molecular level, atoms on the surface interact with the surrounding molecules differently depending on their local atomic arrangement (e.g., facet, edge, corner atoms, and surface defects), leading to remarkable variations in the chemical environment [23]. In addition, surface relaxation and reconstruction influence the chemical reactions at the surface by altering the electronic structures. Collectively, the atomic arrangements and atomic surface reconstructions on the surface form are referred to as surface structures. Studies have shown that the atomic reconstruction of copper oxides has superior active H* utilization. For instance, the rate constant for nitrate removal (0.048 min^{-1}) over Cu_2O/Cu at —1.4 V was 15 times higher than that with Cu foam (0.003 min^{-1}) [24]. Modulation of the surface structure of Cu catalyst includes electrodeposition [25], high-temperature calcination [26], and chemical oxidation [24], each requiring specific conditions. Previous research has explored enhancing electroreduction reactions by introducing a small quantity of noble metals (Au or Ag) into Cu to facilitate the atomic reconstruction of active sites through displacement processes [27,28]. For example, Au/Cu synthesized by galvanic replacement creates electron-deficient Cu active

* Corresponding authors.
E-mail addresses: li_wang_1@tongji.edu.cn (L. Wang), zwwang@tongji.edu.cn (Z. Wang).

https://doi.org/10.1016/j.apcatb.2024.124252
Received 25 March 2024; Received in revised form 18 May 2024; Accepted 27 May 2024
Available online 28 May 2024

sites in a bimetallic system, which promotes the generation of active hydrogen species for NO_3^- hydrogenation [18]. These findings indicate that the interfacial reconstruction on Cu catalyst is a promising approach to optimize the adsorption free energy of hydrogen (ΔG_{H^*}) and thereby enhance electrocatalytic dechlorination.

In this work, we synthesized a Pd/CuO_x cathode by a low atomic reconstruction. Using Cu monometal as a template and a metal precursor (H_2PdCl_4) with a higher reduction potential, the atom in the template is oxidized and the second metal can be reduced and deposited on the template. This process resulted in CuO_x nanoparticles with uniformly dispersed Pd nanoparticles, forming biphasic interfaces. The effects on organochlorine degradation were systematically evaluated under different parameters, including Pd^{2+} dosage, current density, co-anions, pH and flux in the flow-through system. The mechanism of dechlorination and the pathway of 2,4-D degradation were explored. Density functional theory (DFT) calculations confirmed that the synergy between CuO_x and Pd accelerates H_2O dissociation and decreases ΔG_{H^*}. This research provides a new avenue to improve H* generation and remove OCs from wastewater.

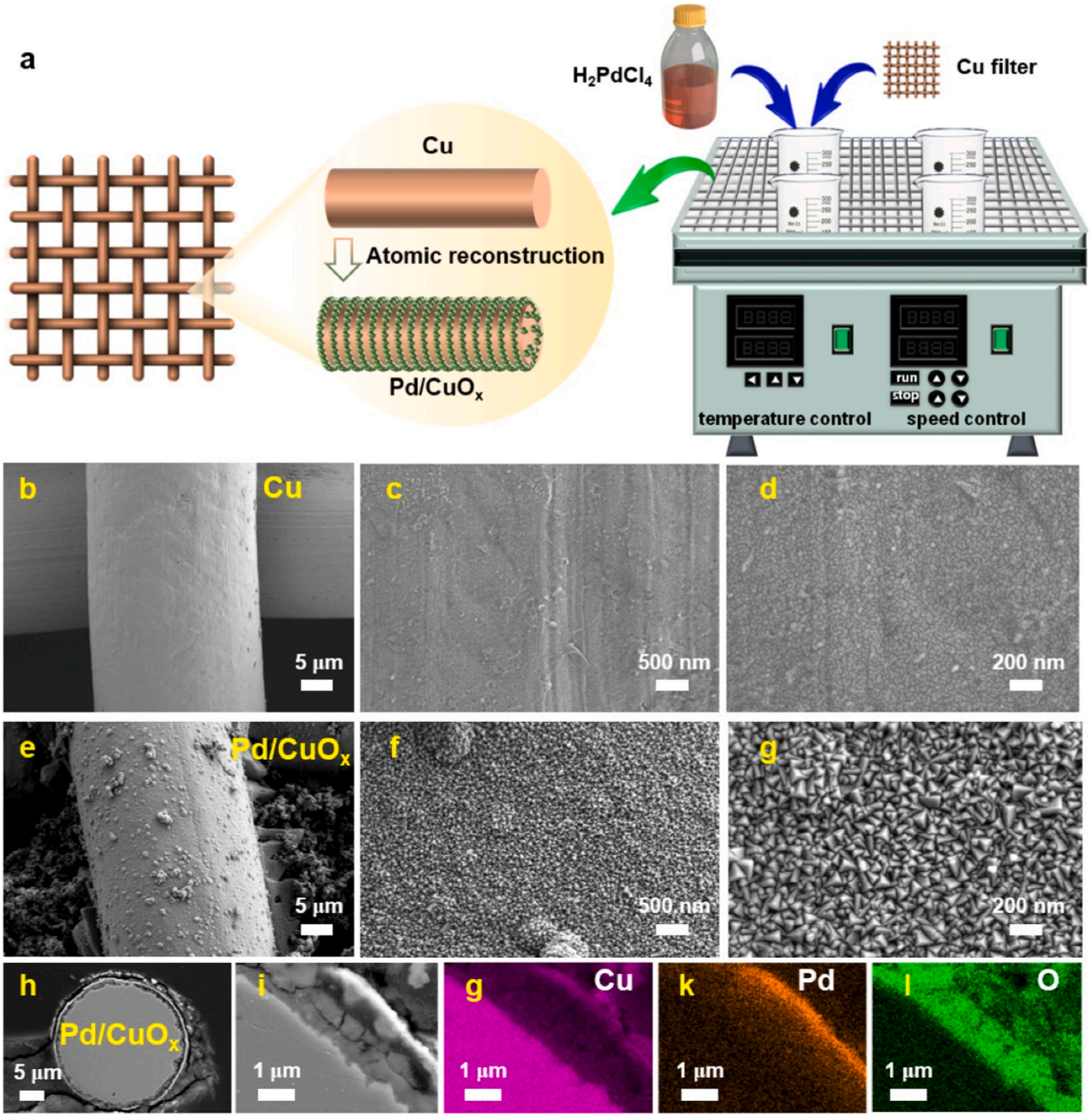

Fig. 1. (a) Schematic illustration of the synthesis processes for Pd/CuO_x electrochemical filter; SEM images of (b)-(d) Cu and (e)-(g) Pd/CuO_x electrodes; (h-i) SEM images of inlaid polished Pd/CuO_x electrodes on the cross-section; (g-l) Elemental mappings of Cu, Pd and O on the Pd/CuO_x electrodes.

2. Material and Methods

2.1. Pd/CuO_x filter fabrication

The Pd/CuO_x filter was first synthesized by a low atomic reconstruction method. Commercial copper meshes (300-mesh, thickness: 0.1 mm) were cut to squares with an area of 9 cm^2 (3 cm × 3 cm). The mesh squares were successively washed with 1 % HCl, ethanol and deionized water, and then dried with nitrogen gas. A 10 mM H_2PdCl_4 stock solution was prepared by dissolving $PdCl_2$ in a solution containing H_2O, 20 mM HCl and 30 mM NaCl under controlled conditions at 60°C. This stock solution was diluted to different concentrations for subsequent reactions. The scheme of the experimental setup is shown in Fig. 1a. Typically, the cleaned Cu-copper mesh was immersed in a mixed solution of 30 mL H_2PdCl_4 solution, oscillating under constant temperature until the solution became transparent. The obtained Pd/CuO_x was then rinsed with deionized water and dried in a vacuum drying oven at 60 °C. Ultrapure water obtained from a Millipore water purification system (Milli-Q) was used in all experiments.

2.2. Batch tests of electrocatalytic decontamination

An electrochemical workstation (CHI 660E) and a DC power (FPS-325 DU, Zhaoxin, China) were used to perform cyclic voltammetry (CV) and constant current electrolysis experiments, respectively. The CV experiments were conducted with a three-electrode cell consisting of a Pt (3 × 3 cm^2) counter electrode, an Ag/AgCl reference electrode, and a Pd/CuO_x (3 × 3 cm^2) working electrode. The constant current electrolysis experiments were performed with a single-chamber electrolysis cell (100 mL), consisting of a Ti (3 × 3 cm^2) counter electrode and a Pd/CuO_x (3 × 3 cm^2) working electrode. Before the experiments, the electrolysis cell was purged with pure N_2 gas for at least 30 min to exclude the interference of oxygen. The system was magnetically stirred at a rate of 150 rpm. The concentrations of 2,4-D reduction were determined to investigate the electrochemical process of halogenated organic compound reduction at different current densities. In the batch mode, 40 μM of the halogenated organic compounds and 50 mM Na_2SO_4 were added to the electrolysis cell. Each set of batch tests was conducted in triplicate.

The electrical energy per order of 2,4-D removal (E_{EO}, kWh m^{-3}) and the theoretical energy consumption of 2,4-D removal (E_t, kWh m^{-3}) in the batch tests were calculated by the following equations [29]:

$$R = \frac{C_0 - C_t}{C_0} \times 100\% \quad (1)$$

$$-k_{app}t = \ln\left(\frac{C_t}{C_0}\right) \quad (2)$$

$$E_{EO} = \frac{UIt}{V \log(C_0/C_t)} \quad (3)$$

$$E_t = \frac{UIln(1-R)}{k_{app}V} \quad (4)$$

where U is the cell potential (V), I is the current (A), t is the operating time (h), C_0 is the 2,4-D concentration in the feed solution (mg L^{-1}), C_t is the concentration of 2,4-D at time t (mg L^{-1}), R is 2,4-D removal efficiency, k_{app} is the rate constant (h^{-1}), and V is the solution volume (L).

2.3. Continuous-flow 2,4-D removal tests in an electrochemical device

Continuous-flow tests for the removal of 2,4-D were conducted in a customized plexiglass device (dimensions = 3 × 3 × 1 cm^3, see Fig. S1 for details). Inside the device, a Ti mesh (3.5 × 3.5 cm^2) and an as-prepared filter (3.5 × 3.5 cm^2) were used as the anode and cathode, respectively. The distance between the anode and cathode was set at 10 mm. A solution containing 40 μM of 2,4-D and N_2-saturated 50 mM Na_2SO_4 passed through the electrochemical filter at a flux of 20–120 L m^{-2} h^{-1}. The solution was pumped through the mesh electrodes in the direction from the cathode to the anode while applying a constant current across the electrodes.

2.4. Analytical methods

The surface morphology and element distribution on the Pd/CuO_x were characterized by field emission scanning electron microscopy (SEM, Zeiss Gemini 300, Germany). X-ray diffraction (XRD, Bruker D8, Cu Kα ($\lambda = 0.15406$ nm), Germany) was conducted to examine the phase structure. The chemical states of the component elements on the surface were investigated with X-ray photoelectron spectroscopy. The surface state and elemental composition analyses were conducted using X-ray photoelectron spectroscopy (XPS, ESCALAB 250Xi, America). Electrochemical measurements were performed using an electrochemical workstation (CHI 660E) in a conventional three-electrode system, with a platinum sheet as the counter electrode and an Ag/AgCl electrode as the reference electrode. Electron spin resonance (ESR) was acquired in a single-chamber reactor without contaminants. The 5,5-dimethyl-1-pyrroline N-oxide (DMPO) was a spin-trapping agent for H* and hydroxyl radicals. The tert-butyl alcohol (TBA) was used as a scavenger to explore the contribution of H* on the 2,4-D removal.

The concentrations of 2,4-D, 4-chloroaniline (PCA), 4-chlorophenol (4-CP) and 4-chlorophenoxyacetic acid (4-CPA) were measured with high-performance liquid chromatography (HPLC, Therma Scientific, Vanquish) (details in Text S1). The detection methods for intermediates generated during 2,4-D degradation were depicted in Text S1. The toxicity assessment was shown in Text S2. The leaching mass of Pd and Cu was analyzed using inductively coupled plasma mass spectrometry (ICP-MS, PerkinElmer NexION 300X).

2.5. DFT calculations

The DFT calculations were performed using the Vienna ab initio Simulation Program (VASP) to calculate the predicted density of states of the active metal sites, the adsorption energy for H_2O and the free energy of the potential pathway for the H* reaction. The Gaussian 09 W and Multiwfn 3.8 software packages were used to perform DFT simulations to determine the sites of pollutant molecules that were most likely to be attacked during the degradation process. Text S3 provides more details on the theoretical calculations.

3. Results and Discussion

3.1. Characterization of Pd/CuO_x electrodes

We characterized the surface morphology of the electrochemical filters of Cu and Pd/CuO_x by SEM. The pristine Cu exhibited a cylindrical skeleton with very clean and smooth surfaces (Fig. 1b-d). After atomic reconstruction, dense conical nanoparticles were coated on the surface (Fig. 1e-g). In the cross-section morphology of Pd/CuO_x, the energy-dispersive spectroscopy (EDS) mapping showed that the Pd particles were homogeneously dispersed on the filter surface (Fig. 1h-j), and the Pd doping increased the surface roughness and surface-specific area of Cu mesh.

The crystalline structure and elemental chemical states of the Pd/CuO_x cathode were characterized by XRD and XPS. The as-prepared cathode revealed the distinct diffraction peaks of the (111), (200) and (220) planes at $2\theta = 43.2^o$, 50.4^o and 74.1^o, respectively (Fig. 2a). These observations are consistent with the values found in the standard card of Cu (JCPDS Card no.04–0836) [26]. Analysis of the XRD pattern revealed that additional peaks at 37.0^o, 42.6^o and 47.2^o attributed to Cu_2O, and two peaks at 32.5^o and 56.7^o correspond to CuO [26,30]. Furthermore,

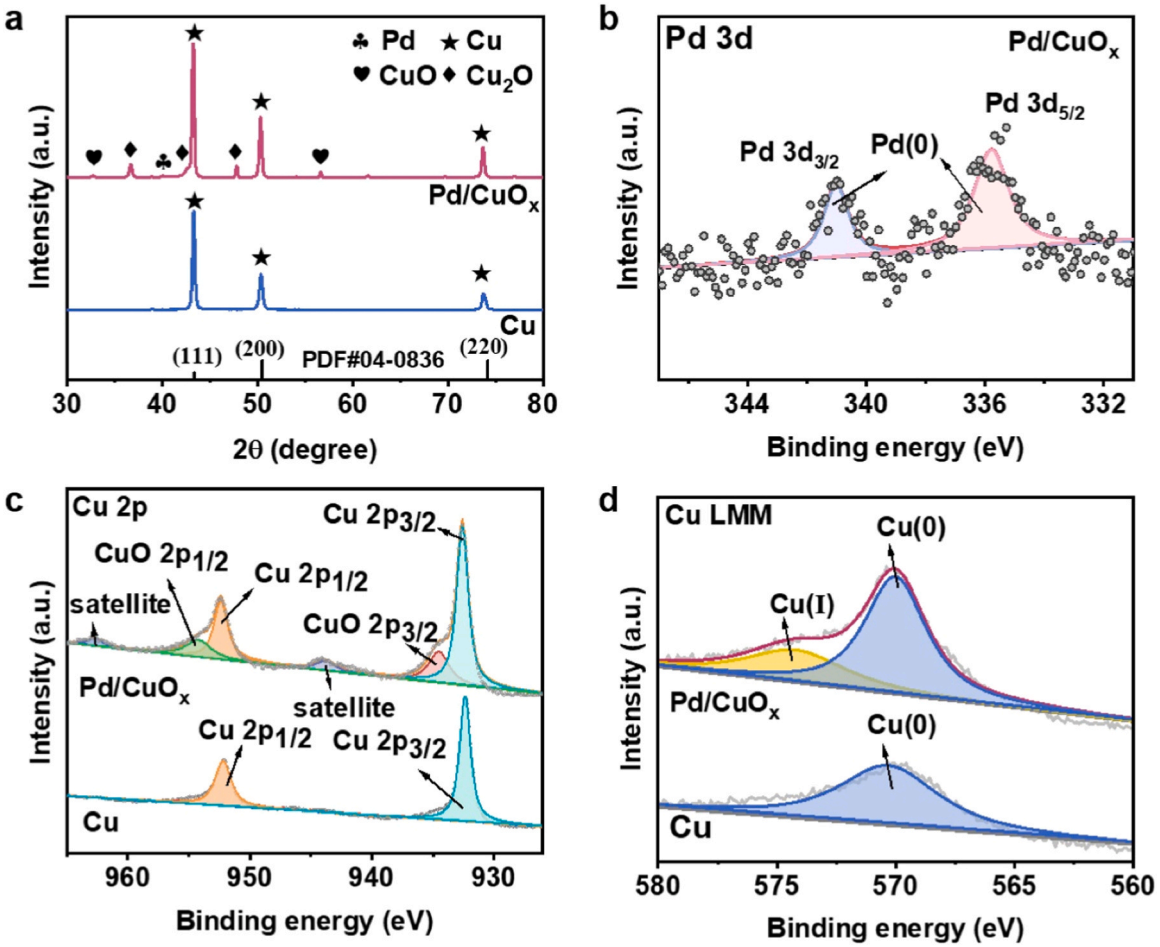

Fig. 2. (a) XRD patterns for the Cu and Pd/CuO_x electrode; (b) high-resolution XPS spectra of Pd 3d for Pd/CuO_x electrode; (c) High-resolution XPS spectra of Cu 2p and (d) Cu LMM spectra for the Cu and Pd/CuO_x electrode.

the XPS spectra (Fig. 2b) displayed two peaks at 335.9 eV and 341.1 eV for Pd 3d, which can be ascribed to Pd $3d_{5/2}$ and Pd $3d_{3/2}$, respectively, indicating the presence of Pd(0) on the Pd/CuO_x [31]. Cu 2p XPS spectra exhibited major peaks at approximately 932.8 eV and 952.5 eV, which were assigned to the $2p_{3/2}$ and $2p_{1/2}$ of Cu(0), respectively [32,33]. The Cu $2p_{3/2}$ peak was deconvoluted into two subpeaks at 934.5 eV and 932.6 eV, respectively (Fig. 2c), indicating Cu(II) and Cu(0) are in mixed valence states [28,34]. The Cu LMM spectra (Fig. 2d) revealed

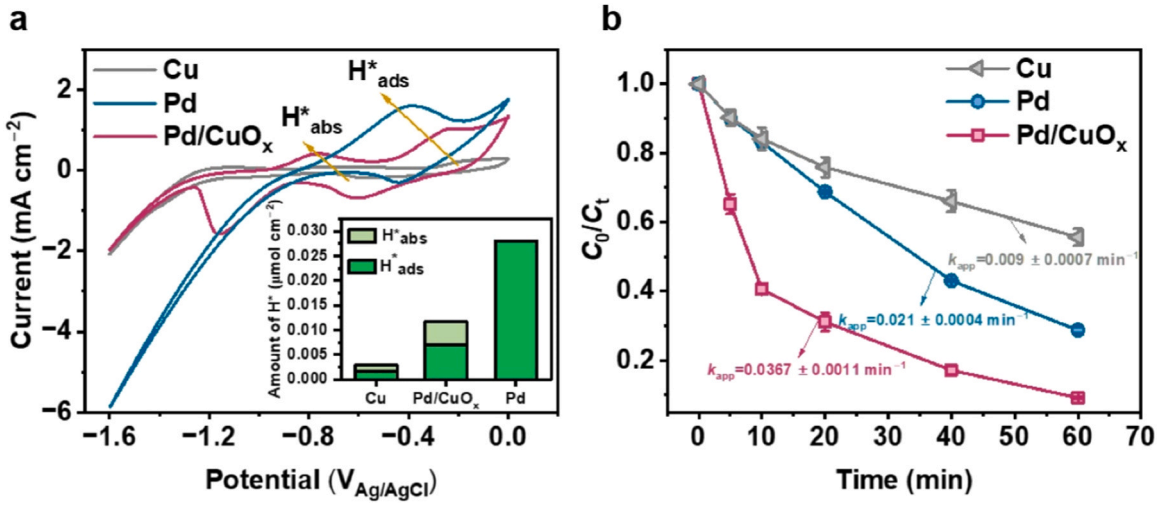

Fig. 3. Cyclic voltammograms of (a) Cu, Pd and Pd/CuO_x in the electrolyte. The insert is the amount of different H* species on the catalysts, estimated from the oxidation charges based on the distinct voltametric behaviors. Conditions: Pt as anode, N_2-saturated 50 mM Na_2SO_4, scan rate = 10 mV s^{-1}; (b) Electrocatalytic performance of Cu, Pd and Pd/CuO_x on the 2,4-D removal. Conditions: Ti as anode, N_2-saturated 50 mM Na_2SO_4, 40 μM 2,4-D, the current density of 4 mA cm^{-2}, magnetic stirring speed of 150 rpm.

characteristic Auger peaks of Cu(0) at 570.3 eV and Cu(I) at 574.2 eV after Pd doping. Overall, the comprehensive analysis indicated simultaneous phases of Cu, Cu_2O, and CuO, suggesting the atomic transformation from Cu to CuO/Cu_2O during the atomic reconstruction process. The displacement process offered three main advantages: i) conversion of Cu into polyhedral Cu-based nanoparticles through a chemical oxidation reaction; ii) promotion of the formation of an active Pd(0) phase; iii) reduction in the use of noble metals and fabrication cost of the electrode.

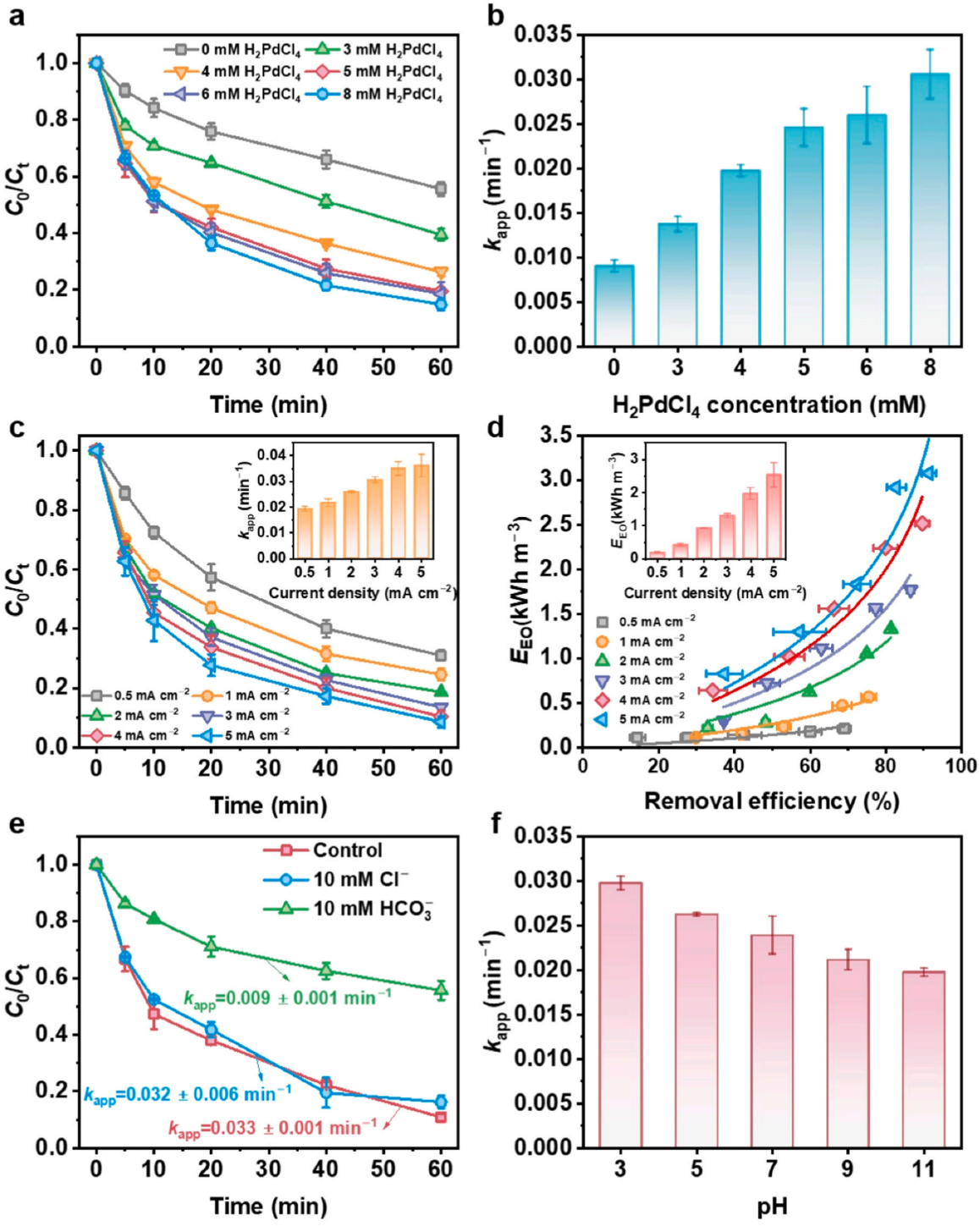

Fig. 4. (a) 2,4-D degradation as a function of time and (b) corresponding rate constants at different Pd^{2+} dosages. Conditions: Ti as anode, N_2-saturated 50 mM Na_2SO_4, 40 μM 2,4-D, the current density of 2 mA cm^{-2}, magnetic stirring speed of 150 rpm in a batch; (c) 2,4-D degradation as a function of time at different current densities, the inset figure shows the relationship between current density and rate constant; (d) Scatter plot and fitted curve of the relationship between degradation efficiency and energy consumption. The points are determined by the energy consumption at 5, 10, 20, 40, and 60 min calculated from Eq. (3). The lines are the fitted curve of the relationship between removal efficiency and energy consumption based on the theoretical energy consumption following Eq. (4). The inset figure shows the relationship between current density and energy consumption in 60 min; (e) 2,4-D degradation as a function of time in presence of bicarbonate and chloride ions; (f) The rate constants of 2,4-D at various pH levels. Conditions: Ti as anode, N_2-saturated 50 mM Na_2SO_4, 40 μM 2,4-D, magnetic stirring speed of 150 rpm.

3.2. Enhanced H^*_{ads} provision capacity of Pd/CuO_x

The electrocatalytic performance of the Pd, Cu and Pd/CuO_x electrodes for the generation and storage of active hydrogen species was investigated by cyclic voltammetry in a N_2-saturated 50 mM Na_2SO_4 solution. Fig. 3a shows that two oxidation peaks were observed at potential scans in the range of —0.1 to —0.4 $V_{Ag/AgCl}$ and −0.6 to −0.8 $V_{Ag/AgCl}$. These peaks corresponded to the adsorbed H* on the metal surface (H^*_{ads}) and the absorbed H* by the formation of the metal—H* bonds (H^*_{abs}) [35], respectively. H^*_{ads} may be consumed by the recombination of two atomic H (Tafel reaction), potentially reducing its contribution to dechlorination [14]. In contrast, H^*_{abs} might form stable Pd−H bonds against the HER, contributing to excellent performance in cathodic dechlorination [36]. Furthermore, the estimation of the different hydrogen species based on the oxidation charges showed that the Pd/CuO_x electrode had a higher relative abundance of H^*_{ads} (0.007 μmol cm^{-2}) and H^*_{abs} (0.0046 μmol cm^{-2}) compared to the Cu electrode (0.0016 and 0.0012 μmol cm^{-2}). This observation indicates a superior catalytic activity of the Pd/CuO_x electrode in the generation of H* species. The 2,4-D removal efficiency of Pd/CuO_x in a batch system was 90.8 %, an increase of 46 % compared to pristine Cu at the same operating conditions (Fig. 3b). Despite a higher amount of H^*_{ads} with Pd (0.028 μmol cm^{-2}), the 2,4-D removal efficiency of Pd (71.2 %) showed significantly lower activity. This discrepancy is attributed to the massive accumulation of H* at the active sites, which facilitates the formation and release of hydrogen gas [11]. In summary, these results confirm that the exceptional electrocatalytic ability of Pd/CuO_x in both generating and storing H* species.

3.3. Effects of main factors on electrocatalytic performances over Pd/CuO_x

We first investigated the effect of Pd concentration. The electrochemical degradation experiments were conducted in the batch mode under different Pd^{2+} dosages. As shown in Fig. 4a, the removal efficiency of 2,4-D increased significantly from 60.5 % to 80.5 % under a fixed current density of 2 mA cm^{-2}, as H_2PdCl_4 dosage increased from 3 mM to 5 mM. However, further increasing the dosage of H_2PdCl_4 to 6 mM and 8 mM showed a negligible effect on the 2,4-D removal. To quantitatively understand the reaction kinetics of 2,4-D degradation, the rate constants of pseudo-first-order kinetics (k_{app}) were calculated (Fig. 4b). The rate constant achieved with a dosage of 5 mM H_2PdCl_4 (0.025 min^{-1}) was 2.7 times higher than the rate constant at 0 mM H_2PdCl_4 (0.009 min^{-1}). Nevertheless, the difference in degradation rates between 5 mM and 6 mM H_2PdCl_4 was less pronounced, possibly resulting from Pd agglomeration and consequential reduction in the active sites of copper oxide [37,38]. Therefore, 5 mM H_2PdCl_4 was selected for use in subsequent experiments.

The optimal cathode potential or current density is crucial for the electrocatalytic performance of Pd/CuO_x. In principle, it should ensure a sufficient supply of electrons and reactive radicals for dehalogenation while minimizing excessive energy consumption [36,39]. With an increase in current density from 0.5 to 4 mA cm^{-2}, the degradation efficiency and kinetics of Pd/CuO_x improved from 69.0 % to 89.6 %, and from 0.019 min^{-1} and 0.035 min^{-1}, respectively (Fig. 4c). The increase in current resulted in an enhanced generation of H* and thus improved the removal efficiency. The relationship between energy consumption and removal efficiency was further analyzed based on the first-order kinetics [36,39]. The energy consumption increases significantly with the increase in removal efficiency (Fig. 4d). Furthermore, the energy consumption is proportional to the current density. Although there was a slight improvement in the removal efficiency of 2,4-D as the current density increased from 4 to 5 mA cm^{-2}, the energy cost at 5 mA cm^{-2} (2.52 kWh m^{-3}) significantly exceeded that of 4 mA cm^{-2} (1.96 kWh m^{-3}) (see Fig. 4d). Considering both the energy consumption and the removal efficiency, we selected 4 mA cm^{-2} as the optimal current density for subsequent experiments in this study.

The coexistent anions naturally present in actual wastewater might affect the atomic hydrogen generation, and this effect was thus studied. The effects of the chloride and bicarbonate ions on the dechlorination efficiency are illustrated in Fig. 4e. The significant inhibition of 2,4-D removal in the presence of HCO_3^- can be attributed to its tendency to consume H* for the formation of other products [40], while the impact of Cl^- on 2,4-D removal was negligible. Additionally, the pH of the bulk electrolyte can influence H* adsorption and desorption during the dechlorination process [39]. The k_{app} of 2,4-D in electrochemical dechlorination exhibited a decreasing trend with increasing pH (Fig. 4f), which can be attributed to the impact on proton transfer at higher pH levels [36]. Previous studies have indicated that lower pH results in decreased energy barriers, thereby facilitating the conversion from proton to H* based on the entropy-enthalpy relationship of H* conversion [41].

We further investigated the influences of pollutants' charge structure on the catalytic performance of Pd/CuO_x. Fig. 5a-b shows the removal of various chlorinated benzene rings with electron-withdrawing or electron-donating groups over Pd/CuO_x. The electrocatalytic performance exhibited a decreasing trend in the batch system: PCA (98.9 %, 0.081 min^{-1}) > 4-CPA (94.4 %, 0.046 min^{-1}) ≈ 2,4-D (93.2 %, 0.044 min^{-1}) > 4-CP (84.8 %, 0.031 min^{-1}). This result is consistent with previous studies showing that electron-withdrawing groups (e.g., $-OCH_2COOH$) have higher activity for nucleophilic reactions (especially, H*-mediated electrocatalytic dehalogenation) compared to electron-donating groups (e.g., −OH) [36].

Based on the optimized current density determined in the batch test, we conducted experiments in a flow-through mode at 4 mA cm^{-2} under different fluxes (20–120 L m^{-2} h^{-1}). As shown in Fig. 5c, the removal efficiency of 2,4-D exhibited an inverse correlation to the flux. Specifically, 62.9 % of 2,4-D were removed at a flux of 120 L m^{-2} h^{-1}, and the removal efficiency increased to 92.5 % when the flux decreased to 20 L m^{-2} h^{-1}. This phenomenon can be attributed to the prolonged time within the membrane at lower membrane flux, facilitating the contact reaction between the pollutants and the active sites [39].

The stability of the as-prepared Pd/CuO_x cathode was evaluated by continuous operation at a flux of 40 L m^{-2} h^{-1} for 10 h (Fig. 5d). The removal efficiency of 2,4-D remained high between 85 % and 93 % throughout the operation. Furthermore, the leaching of Pd and Cu ions was found to be below 10 μg L^{-1} and 100 μg L^{-1}, respectively. This indicates that the Pd/CuO_x electrode can sustain a long-term operation.

Additionally, we compared the performance of the Pd/CuO_x for 2,4-D removal with electrodes reported in literature [40,42–49]. As shown in Table 1, the Pd/CuO_x cathode in this work outperformed most cathodic materials, exhibiting a lower required Pd loading compared to other Pd-based catalysts in the literature. Note that the catalytic rate constant of Pd/CuO_x increased by 1.2, 4.8, 7.7 and 14.8 times compared with that of Co_1Cu_p-NC [49], Pd_1Cl_3 [43], Pd/Ni foam [42] and nTiN doped Pd/Ni foam [45], respectively. The synergistic cooperation of CuO_x and Pd can significantly accelerate H_2O dissociation and H* radical generation, which underscores the prospects of the Pd/CuO_x catalyst in effectively removing organic chlorides.

3.4. 2,4-D degradation products and toxicity assessment

LC-MS analyses were performed at different time intervals to evaluate the degradation process of 2,4-D (Fig. S2). The chromatogram showed a peak corresponding to the original 2,4-D at a retention time of 14.53 min. At the same time, the peak area of 2,4-D decreased stepwise by 96 %, which corresponds well with the rapid decrease in 2,4-D concentration (Fig. S3a). The possible molecular structures of the resultant products are listed in Table S1 and Fig. S4-S5. The transformation of 2,4-D was facilitated through a dechlorination reaction pathway (Fig. 6a). In the pathway I, the C−O bond on the phenoxy group of 2,4-D was attacked by H*, leading to the formation of 2,4-

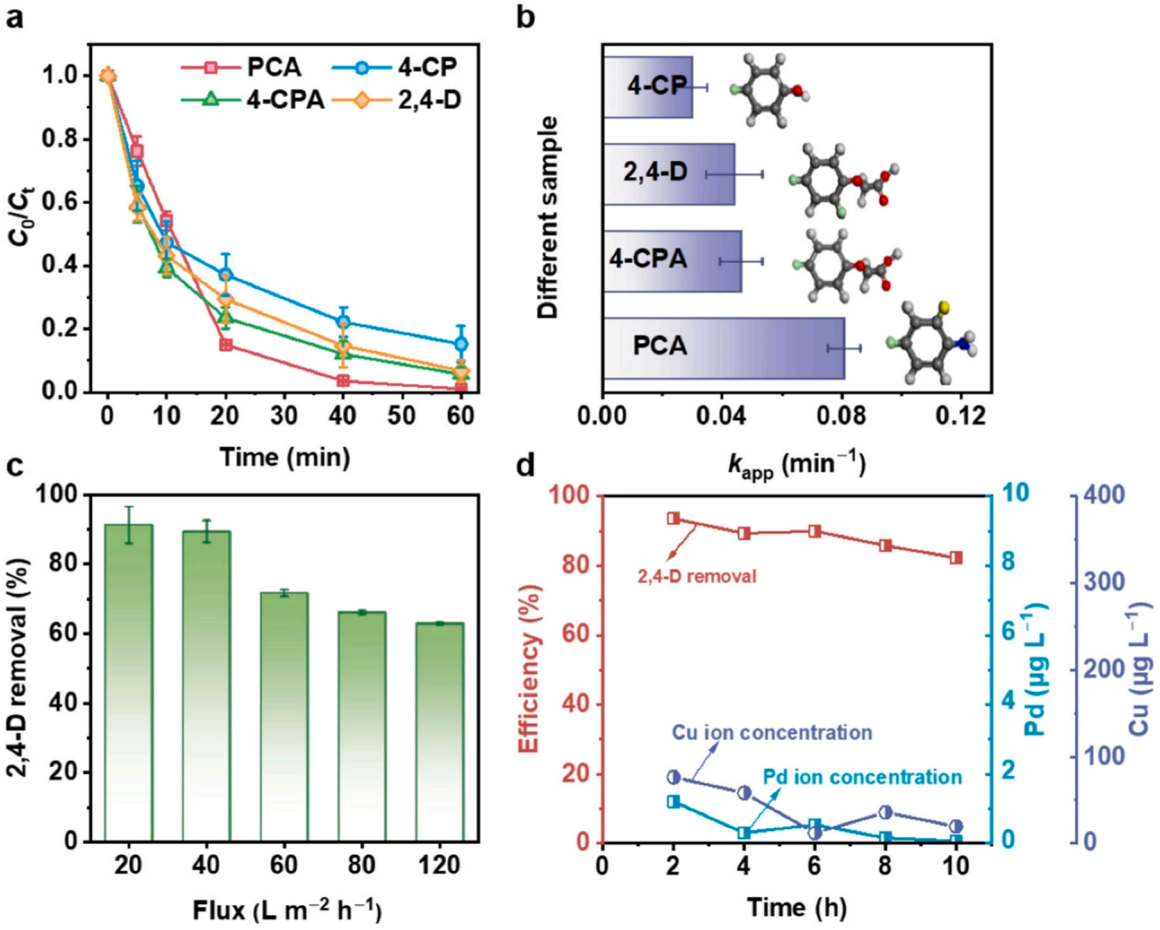

Fig. 5. (a) Removal efficiency and (b) rate constant of different pollutants in the batch system. Conditions: Ti as the anode, Pd/CuO_x as the cathode, N_2-saturated 50 mM Na_2SO_4, 40 μM pollutant concentration, current density of 4 mA cm^{-2}; (c) 2,4-D removal using Pd/CuO_x while varying water flux in a flow-through membrane; (d) 2,4-D removal efficiency and leaching of metal ions using Pd/CuO_x at a flux of 40 L m^{-2} h^{-1} for 10 h. Conditions: Ti as the anode, Pd/CuO_x as the cathode, N_2-saturated 50 mM Na_2SO_4, 40 μM 2,4-D, current density of 4 mA cm^{-2}.

Table 1
Comparison of the electrocatalytic performance for 2,4-D removal using the previously reported materials.

Cathode	Current or Cell voltage	Pd loading (mg cm^{-2})	C_0 (mM)	Time (min)	Removal (%)	Atmosphere	k_{app} (min^{-1})	Ref
Pd/Ni foam	1.7 mA cm^{-2}	16.79	0.226	240	71	N_2	0.0088	[42]
Pd/Ag(r)	4.2 mA cm^{-2}	~0.9	25	60	92.3	H_2	/	[44]
nTiN doped Pd/Ni foam	1.7 mA cm^{-2}	~0.9	0.226	120	~100	without N_2	0.0046	[45]
CD-Pd/foam-Ni	1.5 mA cm^{-2}	52.9	0.226	180	79	without N_2	/	[46]
Pd_1Cl_3	−0.65 V	/	0.226	120	81.4	without N_2	0.014	[43]
Pd-NiMOF/Ni	−1.5 V	4.59	0.045	240	99.8	without N_2	/	[40]
Pd/$NiCo_2O_4$/Ni-foam	−1.5 V	4.01	0.045	90	~100	N_2	/	[47]
Co_1Cu_p-NC	−0.5 V	/	0.09	80	89.2	N_2	0.0575	[49]
Pd-Co_3O_4/Ni foam	1.5 mA cm^{-2}	/	0.226	120	94.2	without N_2	/	[48]
Pd/CuO_x	4 mA cm^{-2}	1.77	0.04	60	97	N_2	0.068	This work

dichlorophenol (P162, m/z = 162). From P162, 4-chlorophenol (P128–1, m/z = 152) and 2-chlorophenol (P128–2, m/z = 152) were formed by H* attack and removal of the Cl^- located in para or ortho position [40]. In the pathway II, the direct interaction of 2,4-D (m/z = 219) with the H^*_{ads} on the metal catalyst resulted in stepwise Cl^- release and H addition, which transformed into 4-chlorophenoxyacetic acid (P186–1, m/z = 186) or 2-chlorophenoxyacetic acid (P186–2, m/z = 186) [50]. This process further progressed to the generation of phenoxyacetic acid (P152, m/z = 152).

Phytotoxicity assessment was performed on mung beans (*Vigna radiata*) to evaluate the toxicity of 2,4-D and its intermediates before and after exposure to the electrocatalytic system solution. Fig. S6 shows that the addition of 2,4-D resulted in a significant inhibition of seed germination compared to the control (50 mM Na_2SO_4). The shoot and root length of germinating seeds decreased from 1.97 cm to 0.38 cm (i.e., a ~81 % decrease). After treatment with the electrocatalytic system, the length of germinating seeds increased from 0.38 cm to 0.97 cm (an increase of 61 %), indicating a reduction in toxicity when 2,4-D was treated with the Pd/CuO_x cathode. This observation was consistent with the decreased peak area of 2,4-D and its intermediates (Fig. S3). Nevertheless, the electrocatalytic degradation of 2,4-D did not completely eliminate the toxicity. This can be attributed to the possible generation of toxic intermediates during the degradation process. Based on the molecular structure of the intermediates, the molecular toxicity was evaluated in Fig. 6b-c using the quantitative structure-activity relationship (QSAR) prediction. The acute toxicity LC_{50} of fathead

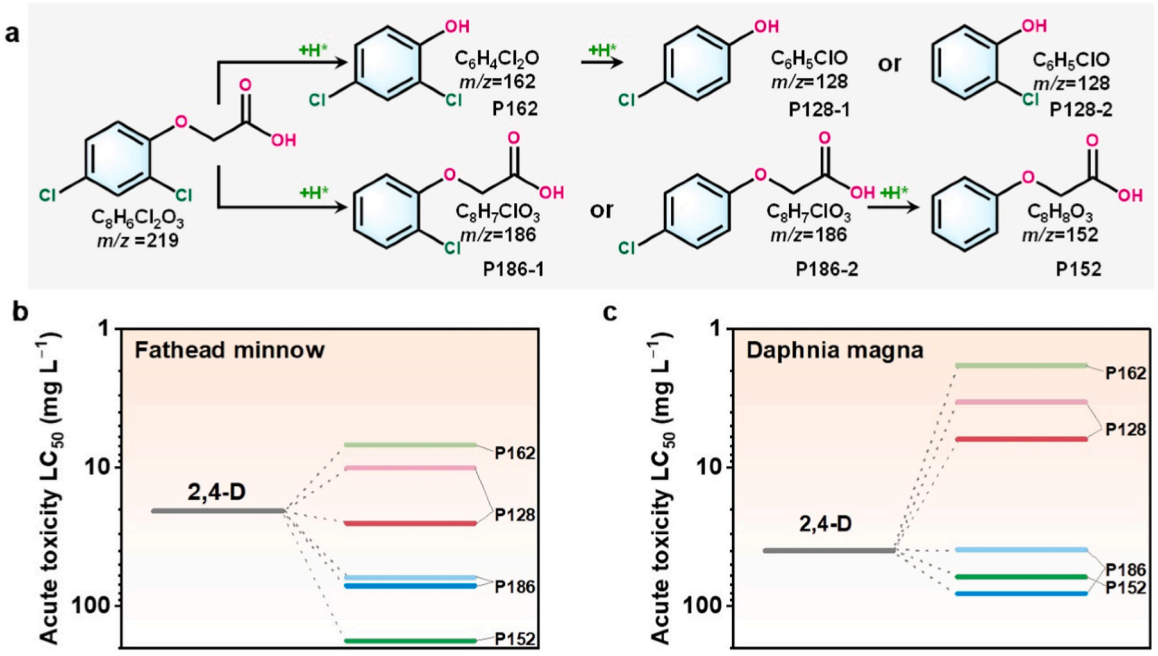

Fig. 6. (a) The possible degradation pathway of 2,4-D using Pd/CuO_x cathode; The acute toxicity of (b) Fathead minnow and (c) Daphnia magna 2,4-D and its intermediates. The acute toxicity LC_{50} of compounds was evaluated by QSAR prediction using T.E.S.T. with the consensus method.

minnow for 2,4-D was 20.58 mg L^{-1}. In comparison, the fathead minnow values for P186 (80.74 and 39.16 mg L^{-1}) and P152 (61.41 mg L^{-1}) were higher than those of the initial 2,4-D (Fig. 6b), suggesting that the potential products are less toxic than 2,4-D. Moreover, the acute toxicity LC_{50} of Daphnia magna values show that most products have lower toxicity to Daphnia magna than 2,4-D (Fig. 6c). These results are consistent with the phytotoxicity analysis of the degradation of 2,4-D, demonstrating the significance of the electrocatalytic process in water remediation.

3.5. *Identification and active species in the Pd/CuO_x system*

Dissolved oxygen in the feed water potentially competes with electrons and atomic H* in the dehalogenation reaction[14,51]. It was found that the reaction rate constant under N_2 conditions was 1.8 times higher than that under open-air conditions (Fig. 7a). Therefore, nitrogen gas is usually purged in the solution before and during electrolysis.

Scavenging experiments were performed to investigate the dominant active species in the reaction solution. Given that t-BuOH can react with H* and generate inert 2-methyl-2-propanol radicals, t-BuOH is commonly used as a quenching agent to trap active H* in electrocatalytic hydrodechlorination [31]. As shown in Fig. 7b, the 2,4-D removal significantly decreased from 96.7 % to 27.5 % after adding 400 mM TBA, when the TBA concentration increased in the N_2-saturated electrolyte. However, the presence of TBA did not completely inhibit the degradation of 2,4-D, indicating that direct electron transfer is likely involved in electrochemical dehalogenation in the system.

ESR analysis using DMPO as a spin-trapping reagent was performed in the Pd/CuO_x system. In Fig. 7c, nine characteristic peaks of DMPO-H* were observed in the electroreductive system with the Pd/CuO_x cathode [52]. Additionally, a typical four-line ESR spectrum of DMPO-•OH with a low intensity of 1:2:2:1 was recorded near the anode Ti (Fig. S7). Although the relative intensities of DMPO-H* adducts could not provide a quantitative correlation, a stronger intensity can generally be qualitatively interpreted as a higher concentration of H* than •OH. This indicates that atomic H* plays a dominant role in the removal of 2,4-D.

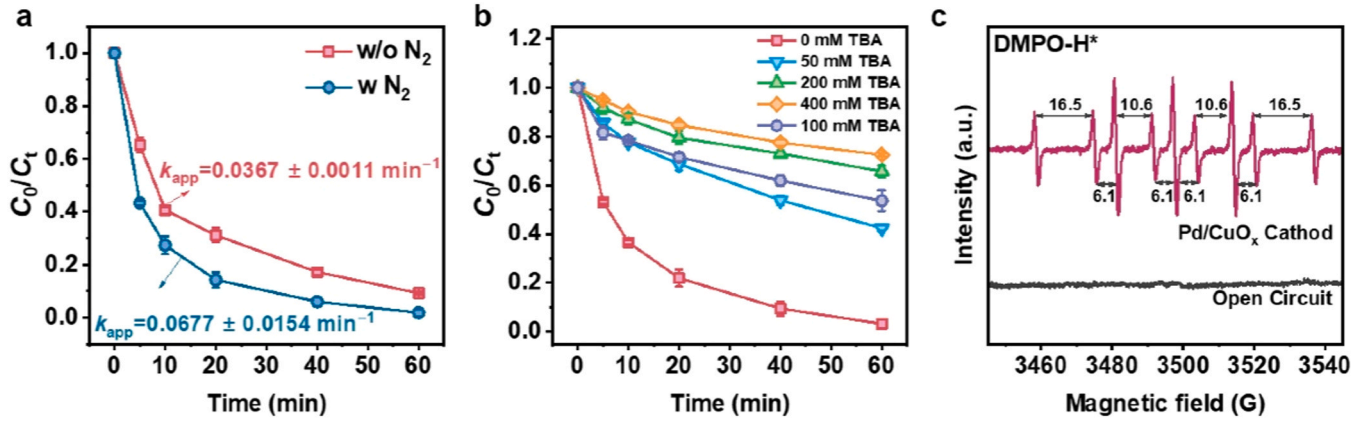

Fig. 7. (a) 2,4-D degradation with and without N_2 purging; (b) 2,4-D h degradation at varying concentrations of t-BuOH; (c) EPR spectra of Pd/CuO_x with DMPO as the probe. Conditions: Ti as the anode, Pd/CuO_x as the cathode, N_2-saturated 50 mM Na_2SO_4, 40 μM 2,4-D, a current density of 4 mA cm^{-2}.

3.6. Mechanism of enhanced catalyst activity on the Pd/CuO_x electrode

DFT calculations were performed to elucidate the role of Pd/CuO_x in facilitating H* formation via H_2O dissociation, with a focus on H* adsorption on Pd/CuO_x. The HER pathway in alkaline conditions involves the initial dissociation of H_2O into H* and OH*, followed by the subsequent generation of H_2 [22,53]. Model systems, including Pd, Pd/Cu, Pd/CuO, and Pd/Cu_2O, were established to investigate the optimized adsorption configurations of OH*-H* and H* (Fig. 8a and Fig. S8). The free energy of water dissociation (ΔG_{H2O}) revealed that Pd/Cu_2O (0.22 eV) was more effective in H_2O dissociation compared to Pd (0.51 eV) and Pd/Cu (0.37 eV) (Fig. 8b). This indicates a higher efficiency of Pd/Cu_2O in facilitating H_2O dissociation, where H_2O adsorption on Cu_2O surfaces involves O atoms bonding at Cu sites and H atoms forming hydrogen bonds with Cu_2O's lattice O [54]. Furthermore, the ΔG_{H^*} value, critical for H formation, showed that Pd/CuO, despite its higher efficacy in H_2O dissociation, had a rate-determining step (RDS) in generating H* from OH*-H*. The energy barrier for this generation (ΔG_{H^*} = 0.18 eV) was higher than that observed in Pd and Pd/Cu systems.

We propose a mechanism for Pd/CuO_x by integrating ESR and DFT results (Fig. 8c). The excellent OCs removal rate of Pd/CuO_x was due to the synergistic effect of CuO_x and Pd, which optimized the dissociation of water and enhanced the free adsorption energy of hydrogen. In the adsorbed-hydrogen-mediated pathway, the electrons first reduce the adsorbed H_2O in an aqueous solution through a proton reduction step, *i.e.*, the Volmer reaction [55]. Subsequently, surface-adsorbed H^*_{ads} species on the metal surface act as intermediates, facilitating the activation and cleavage of C—Cl bonds. In contrast to Pd/Cu, CuO_x exhibits a stronger water dissociation ability, leading to an increased production of H* species. The resulting H* intermediates migrate towards low-valence Pd atoms, forming stable Pd—H bonds in Pd/CuO_x. Consequently, the synergistic interaction between the dominant Cu (I)/(II) configurations and the Pd(0) state enhances hydrogen generation, thereby improving the removal of OCs.

4. Conclusions

In this work, effective Pd/CuO_x electrocatalysts were developed by a simple atomic reconstruction method. The Cu atom in the template was oxidized to form CuO_x, while the Pd metal could be reduced and deposited on the template. The interaction between Pd and Cu effectively promoted the formation of Cu(I)/(II) and Pd(0) states. The electrocatalytic performance of the Pd/CuO_x cathode showed fast reaction kinetics and remarkable efficiency in the removal of organochlorine compounds. In particular, the removal (rate constant) of PCA, 4-CP, and 2,4-D were 99 % (0.08 min^{-1}), 85 % (0.03 min^{-1}), and 94 % (0.04 min^{-1}), respectively, at an applied current density of 4 mA cm^{-2}. CV analyses revealed that the increased amount of H* over Pd/CuO_x contributed to a 46 % improvement in the removal of 2,4-D compared with the pristine Cu cathode. The analysis of acute toxicity and phytotoxicity assessment revealed that the degradation products have a lower ecological risk compared to organic chlorides, supporting the significance of the electrocatalytic dechlorination process in water remediation. The scavenging experiments and ESR analyses underpinned the involvement of H*-mediated reduction in the electrocatalytic dechlorination process. DFT calculations provided insights into the synergistic effect of CuO_x and Pd, illustrating a significant acceleration of H_2O dissociation as well as a reduction of the hydrogen adsorption energy. This led to a thermodynamically favorable equilibrium between H* adsorption and desorption, elucidating the mechanistic basis for the observed enhanced electrocatalytic activity.

CRediT authorship contribution statement

Zhiwei Wang: Writing – review & editing, Supervision, Funding acquisition. **Li Wang:** Writing – review & editing, Funding acquisition, Conceptualization. **Yun Guo:** Writing – original draft, Methodology, Investigation, Data curation, Conceptualization. **Yang Li:** Investigation, Conceptualization. **Wei Shi:** Investigation, Data curation. **Yuan Jia:** Investigation.

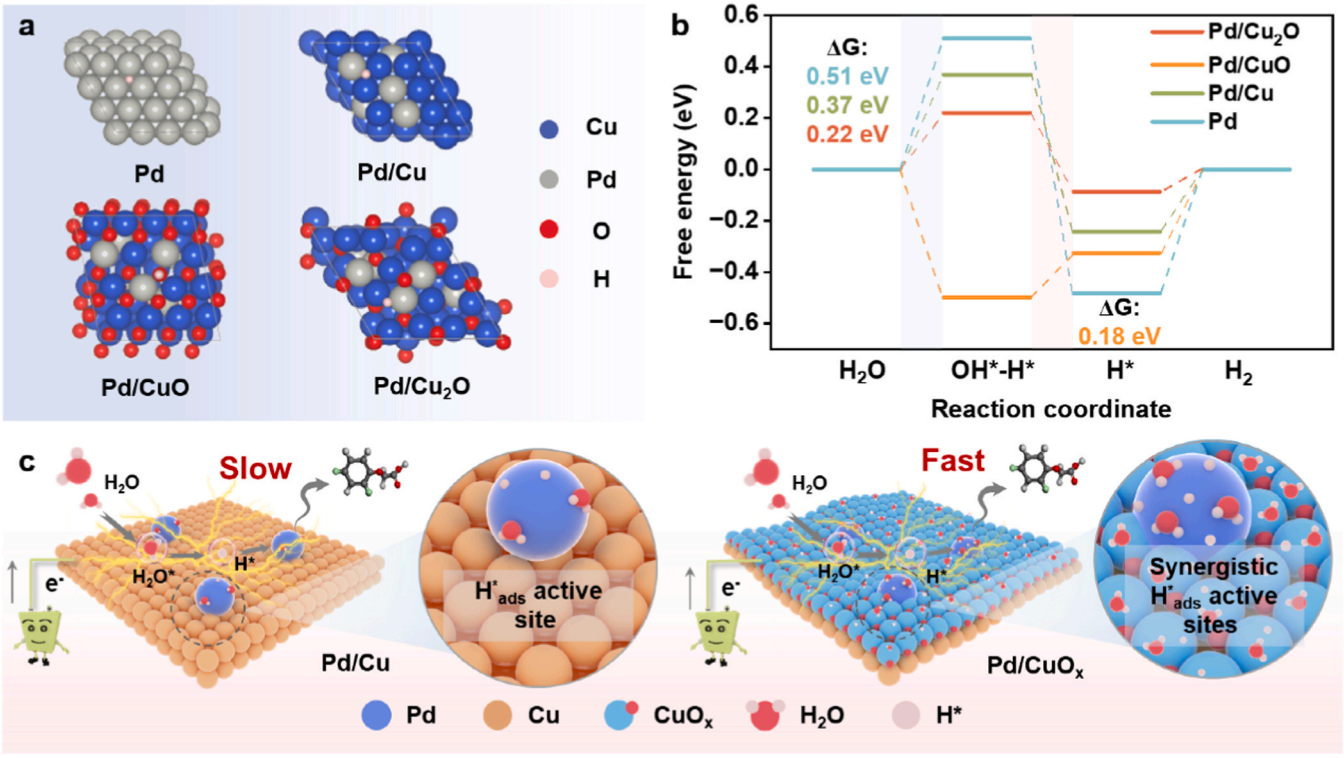

Fig. 8. (a) The optimal H* absorption configuration for Pd, Pd/Cu, Pd/CuO and Pd/Cu_2O; (b) The corresponding free energy diagram for HER of Pd, Pd/Cu, Pd/CuO and Pd/Cu_2O; (c) Schematic diagram of synergistic interaction over Pd/CuO_x.

Declaration of Competing Interest

The authors declare that they have no known competing financial interests or personal relationships that could have appeared to influence the work reported in this paper.

Data availability

Data will be made available on request.

Acknowledgements

This work was supported by National Natural Science Foundation of China (Grants 51925806, 52300103, 52300104), and the Fundamental Research Funds for the Central Universities (Tongji University, Grant 22120230244).

Appendix A. Supporting information

Supplementary data associated with this article can be found in the online version at doi:10.1016/j.apcatb.2024.124252.

References

[1] K. Zhao, X. Quan, Y. Su, X. Qin, S. Chen, H. Yu, Enhanced chlorinated pollutant degradation by the synergistic effect between dechlorination and hydroxyl radical oxidation on a bimetallic single-atom catalyst, Environ. Sci. Technol. 55 (20) (2021) 14194–14203, https://doi.org/10.1021/acs.est.1c04943.

[2] M.A. El-Sheikh, T. Hadibarata, A. Yuniarto, P. Sathishkumar, E.M. Abdel-Salam, A. A. Alatar, Role of nanocatalyst in the treatment of organochlorine compounds-a review, Chemosphere 268 (2021) 128873, https://doi.org/10.1016/j.chemosphere.2020.128873.

[3] H.Y. Gao, L. Mao, B. Shao, C.H. Huang, B.Z. Zhu, Why does 2,3,5,6-tetrachlorophenol generate the strongest intrinsic chemiluminescence among all nineteen chlorophenolic persistent organic pollutants during environmentally-friendly advanced oxidation process? Sci. Rep. 6 (2016) 33159 https://doi.org/10.1038/srep33159.

[4] Y. Min, X. Zhou, J.J. Chen, W. Chen, F. Zhou, Z. Wang, J. Yang, C. Xiong, Y. Wang, F. Li, H.Q. Yu, Y. Wu, Integrating single-cobalt-site and electric field of boron nitride in dechlorination electrocatalysts by bioinspired design, Nat. Commun. 12 (1) (2021) 303, https://doi.org/10.1038/s41467-020-20619-w.

[5] M. Gil-Diaz, R.A. Perez, J. Alonso, E. Miguel, S. Diez-Pascual, M.C. Lobo, Iron nanoparticles to recover a co-contaminated soil with Cr and PCBs, Sci. Rep. 12 (1) (2022) 3541, https://doi.org/10.1038/s41598-022-07558-w.

[6] Y. Wang, H. Liu, X. Yang, L. Wang, Aquatic toxicity and aquatic ecological risk assessment of wastewater-derived halogenated phenolic disinfection byproducts, Sci. Total Environ. 809 (2022) 151089, https://doi.org/10.1016/j.scitotenv.2021.151089.

[7] Y. Yang, X. Zhang, J. Jiang, J. Han, W. Li, X. Li, K.M. Yee Leung, S.A. Snyder, P.J. J. Alvarez, Which micropollutants in water environments deserve more attention globally? Environ. Sci. Technol. 56 (1) (2022) 13–29, https://doi.org/10.1021/acs.est.1c04250.

[8] A.A. Kronke, A. Jurkutat, M. Schlingmann, T. Poulain, M. Nuchter, A. Hilbert, H. Kiviranta, A. Korner, M. Vogel, O. Soder, C.G. Bornehag, W. Kiess, Persistent organic pollutants in pregnant women potentially affect child development and thyroid hormone status, Pediatr. Res. 91 (3) (2022) 690–698, https://doi.org/10.1038/s41390-021-01488-5.

[9] Y. Sun, S. Xu, B. Bai, L. Li, Y. Kang, X. Hu, Z. Liao, C. He, Biotemplate fabrication of hollow tubular $Ce_xSr_{1-x}TiO_3$ with regulable surface acidity and oxygen mobility for efficient destruction of chlorobenzene: intrinsic synergy effect and reaction mechanism, Environ. Sci. Technol. (2022), https://doi.org/10.1021/acs.est.2c00270.

[10] Q. Yao, X. Zhou, S. Xiao, J. Chen, I.A. Abdelhafeez, Z. Yu, H. Chu, Y. Zhang, Amorphous nickel phosphide as a noble metal-free cathode for electrochemical dechlorination, Water Res 165 (2019) 114930, https://doi.org/10.1016/j.watres.2019.114930.

[11] J.Y. Lee, J.G. Lee, S.H. Lee, M. Seo, L. Piao, J.H. Bae, S.Y. Lim, Y.J. Park, T. D. Chung, Hydrogen-atom-mediated electrochemistry, Nat. Commun. 4 (2013) 2766, https://doi.org/10.1038/ncomms3766.

[12] J. Xiong, L. Tian, R. Cheng, Promoted catalytic hydrodechlorination for deep degradation of chlorophenols over Rh-La/SiO_2 catalyst, J. Hazard. Mater. 416 (2021) 125913, https://doi.org/10.1016/j.jhazmat.2021.125913.

[13] L.-X. Li, G.-C. Zhang, W.-J. Sun, H.-Y. Zhang, S.-X. Wang, J.-L. Wei, J.-H. He, K. Song, J.-M. Lu, Construction of ultra-small Pt nanoparticles @$Ti_3C_2T_x$ MXene electrocatalyst for efficient and stable electrochemical hydrodechlorination of chloramphenicol, Chem. Eng. J. 433 (2022) 134415, https://doi.org/10.1016/j.cej.2021.134415.

[14] R. Liu, H. Zhao, X. Zhao, Z. He, Y. Lai, W. Shan, D. Bekana, G. Li, J. Liu, Defect sites in ultrathin Pd nanowires facilitate the highly efficient electrochemical hydrodechlorination of pollutants by H^*_{ads}, Environ. Sci. Technol. 52 (17) (2018) 9992–10002, https://doi.org/10.1021/acs.est.8b02740.

[15] J. Li, K. Kong, Efficient palladium catalysts: Application and challenges of electrocatalytic hydrodechlorination technology in wastewater treatment, ChemCatChem 15 (21) (2023), https://doi.org/10.1002/cctc.202300908.

[16] Z. Gu, N. Ni, G. He, Y. Shan, K. Wu, C. Hu, J. Qu, Enhanced hydrosaturation selectivity and electron transfer for electrocatalytic chlorophenols hydrogenation on Ru sites, Environ. Sci. Technol. 57 (43) (2023) 16695–16706, https://doi.org/10.1021/acs.est.3c06669.

[17] A. Borchers, T. Pieler, Programming pluripotent precursor cells derived from Xenopus embryos to generate specific tissues and organs, 26, Genes 1 (3) (2010) 413, https://doi.org/10.3390/genes1030413.

[18] Y. Zhang, X. Chen, W. Wang, L. Yin, J.C. Crittenden, Electrocatalytic nitrate reduction to ammonia on defective Au_1Cu (111) single-atom alloys, Appl. Catal. B Environ. 310 (2022) 121346, https://doi.org/10.1016/j.apcatb.2022.121346.

[19] S. Qin, C. Lei, X. Wang, W. Chen, B. Huang, Electrocatalytic activation of organic chlorides via direct and indirect electron transfer using atomic vacancy control of palladium-based catalyst, Cell Rep. Phys. Sci. 3 (1) (2022) 100713, https://doi.org/10.1016/j.xcrp.2021.100713.

[20] F. Shi, J. Li, J. Liang, C. Bao, J.-n Gu, K. Li, J. Jia, Highly dispersed Pd-Cu bimetallic nanocatalyst based on γ-Al_2O_3 combined with electrocatalytic in-situ hydrogen production for nitrate hydroreduction, Chem. Eng. J. 434 (2022) 134748, https://doi.org/10.1016/j.cej.2022.134748.

[21] Y. Chen, C. Feng, W. Wang, Z. Liu, J. Li, C. Liu, Y. Pan, Y. Liu, Electronic structure engineering of bimetallic Pd-Au alloy nanocatalysts for improving electrocatalytic hydrodechlorination performance, Sep. Purif. Technol. 289 (2022) 120731, https://doi.org/10.1016/j.seppur.2022.120731.

[22] J. Wang, B. Guo, J. Sun, Y. Zhou, C. Zhao, Z. Wei, J. Guo, Cooperative hydrogen evolution reaction combining $Cu_{2+1}O$ and Ru active sites, Appl. Catal. B Environ. 324 (2023) 122169, https://doi.org/10.1016/j.apcatb.2022.122169.

[23] S. Yoon, H. Seo, K. Jin, H.G. Kim, S.Y. Lee, J. Jo, K.H. Cho, J. Ryu, A. Yoon, Y. W. Kim, J.M. Zuo, Y.K. Kwon, K.T. Nam, M. Kim, Atomic reconstruction and oxygen evolution reaction of Mn_3O_4 nanoparticles, J. Phys. Chem. Lett. 13 (35) (2022) 8336–8343, https://doi.org/10.1021/acs.jpclett.2c01638.

[24] J. Zhou, F. Pan, Q. Yao, Y. Zhu, H. Ma, J. Niu, J. Xie, Achieving efficient and stable electrochemical nitrate removal by in-situ reconstruction of Cu_2O/Cu electroactive nanocatalysts on Cu foam, Appl. Catal. B Environ. 317 (2022) 121811, https://doi.org/10.1016/j.apcatb.2022.121811.

[25] W. Fu, Z. Hu, Y. Zheng, P. Su, Q. Zhang, Y. Jiao, M. Zhou, Tuning mobility of intermediate and electron transfer to enhance electrochemical reduction of nitrate to ammonia on Cu_2O/Cu interface, Chem. Eng. J. 433 (2022) 133680, https://doi.org/10.1016/j.cej.2021.133680.

[26] Y. Wang, W. Zhou, R. Jia, Y. Yu, B. Zhang, Unveiling the activity origin of a copper-based electrocatalyst for selective nitrate reduction to ammonia, Angew. Chem. Int. Ed. 59 (13) (2020) 5350–5354, https://doi.org/10.1002/anie.201915992.

[27] X. Wang, S. Chen, G. Reggiano, S. Thota, Y. Wang, P. Kerns, S.L. Suib, J. Zhao, Au-Cu-M (M = Pt, Pd, Ag) nanorods with enhanced catalytic efficiency by galvanic replacement reaction, Chem. Commun. 55 (9) (2019) 1249–1252, https://doi.org/10.1039/c8cc08083f.

[28] C. Zhu, L. Zhou, Z. Zhang, C. Yang, G. Shi, S. Zhao, H. Gu, J. Wu, X. Gao, Y. Li, K. Liu, S. Dai, L. Zhang, Dynamic restructuring of epitaxial Au–Cu biphasic interface for tandem CO_2-to-C_{2+} alcohol conversion, Chem 8 (12) (2022) 3288–3301, https://doi.org/10.1016/j.chempr.2022.08.016.

[29] Y. Li, J. Ma, Z. Wu, Z. Wang, Direct electron transfer coordinated by oxygen vacancies boosts selective nitrate reduction to N_2 on a Co-CuO_x electroactive filter, Environ. Sci. Technol. 56 (12) (2022) 8673–8681, https://doi.org/10.1021/acs.est.1c05841.

[30] Y. Zhu, Z. Xu, K. Yan, H. Zhao, J. Zhang, One-step synthesis of CuO–Cu_2O heterojunction by flame spray pyrolysis for cathodic photoelectrochemical sensing of l-cysteine, ACS Appl. Mater. Interfaces 9 (46) (2017) 40452–40460, https://doi.org/10.1021/acsami.7b13020.

[31] D. Huang, D.J. Kim, K. Rigby, X. Zhou, X. Wu, A. Meese, J. Niu, E. Stavitski, J. H. Kim, Elucidating the role of single-atom Pd for electrocatalytic hydrodechlorination, Environ. Sci. Technol. 55 (19) (2021) 13306–13316, https://doi.org/10.1021/acs.est.1c04294.

[32] J. Wang, J.W. Chen, J.D. Chen, H. Zhu, M. Zhang, M.L. Du, Designed synthesis of size-controlled Pt-Cu alloy nanoparticles encapsulated in carbon nanofibers and their high efficient electrocatalytic activity toward hydrogen evolution reaction, Adv. Mater. Interfaces 4 (12) (2017), https://doi.org/10.1002/admi.201700005.

[33] R. Mao, L. Yan, X. Zhao, R. Djellabi, K. Wang, K. Hu, H. Zhu, Insights into co-removal of trichloroacetic acid and bromate by an electroreduction process: competitive reaction mechanism and enhanced atomic H* stabilization, Chem. Eng. J. 429 (2022) 132139, https://doi.org/10.1016/j.cej.2021.132139.

[34] Z.J. Zhang, H.Y. Sun, Y.F. Chen, Y.W. Zhao, M.M. Zhang, C.S. Li, Y. Sun, Z.H. Gao, H.J. Li, Y. Jiang, Modulating p-d orbital hybridization by CuO/Cu nanoparticles enables carbon nanofibers high cycling stability as anode for sodium storage, Rare Met. 42 (12) (2023) 4039–4047, https://doi.org/10.1007/s12598-023-02449-z.

[35] G. Jiang, M. Lan, Z. Zhang, X. Lv, Z. Lou, X. Xu, F. Dong, S. Zhang, Identification of active hydrogen species on palladium nanoparticles for an enhanced electrocatalytic hydrodechlorination of 2,4-dichlorophenol in water, Environ. Sci. Technol. 51 (13) (2017) 7599–7605, https://doi.org/10.1021/acs.est.7b01128.

[36] Y. Guo, Y. Li, Z. Wang, Electrocatalytic hydro-dehalogenation of halogenated organic pollutants from wastewater: a critical review, Water Res 234 (2023) 119810, https://doi.org/10.1016/j.watres.2023.119810.

[37] Z. Zhao, L. Yu, L. Zheng, T. Guo, Z. Lv, S. Song, H. Zheng, TiO_2@PDA inorganic-organic core-shell skeleton supported Pd nanodots for enhanced electrocatalytic

hydrodechlorination, J. Hazard. Mater. 435 (2022) 128998, https://doi.org/10.1016/j.jhazmat.2022.128998.
[38] R. Mao, N. Li, H. Lan, X. Zhao, H. Liu, J. Qu, M. Sun, Dechlorination of trichloroacetic acid using a noble metal-free graphene-Cu foam electrode via direct cathodic reduction and atomic H, Environ. Sci. Technol. 50 (7) (2016) 3829–3837, https://doi.org/10.1021/acs.est.5b05006.
[39] Y. Li, L. Ren, T. Wang, Z. Wu, Z. Wang, Efficient removal of bromate from contaminated water using electrochemical membrane filtration with metal heteroatom interface, J. Hazard. Mater. 446 (2023) 130688, https://doi.org/10.1016/j.jhazmat.2022.130688.
[40] Y. Shen, Y. Tong, J. Xu, S. Wang, J. Wang, T. Zeng, Z. He, W. Yang, S. Song, Ni-based layered metal-organic frameworks with palladium for electrochemical dechlorination, Appl. Catal. B Environ. 264 (2020) 118505, https://doi.org/10.1016/j.apcatb.2019.118505.
[41] J. Rossmeisl, K. Chan, E. Skúlason, M.E. Björketun, V. Tripkovic, On the pH dependence of electrochemical proton transfer barriers, Catal. Today 262 (2016) 36–40, https://doi.org/10.1016/j.cattod.2015.08.016.
[42] K. Zhu, S.A. Baig, J. Xu, T. Sheng, X. Xu, Electrochemical reductive dechlorination of 2,4-dichlorophenoxyacetic acid using a palladium/nickel foam electrode, Electrochim. Acta 69 (2012) 389–396, https://doi.org/10.1016/j.electacta.2012.03.038.
[43] S. Song, Q. Liu, J. Fang, W. Yu, Enhanced electrocatalytic dechlorination of 2,4-dichlorophenoxyacetic acid on in situ prepared Pd-anchored $Ni(OH)_2$ bifunctional electrodes: synergistic effect between H* formation on $Ni(OH)_2$ and dechlorination steps on Pd, Catal. Sci. Technol. 9 (18) (2019) 5130–5141, https://doi.org/10.1039/c9cy01359h.
[44] Y.H. Xu, Q.Q. Cai, H.X. Ma, Y. He, H. Zhang, C.A. Ma, Optimisation of electrocatalytic dechlorination of 2,4-dichlorophenoxyacetic acid on a roughened silver–palladium cathode, Electrochim. Acta 96 (2013) 90–96, https://doi.org/10.1016/j.electacta.2013.02.068.
[45] C. Sun, Z. Lou, Y. Liu, R. Fu, X. Zhou, Z. Zhang, S.A. Baig, X. Xu, Influence of environmental factors on the electrocatalytic dechlorination of 2,4-dichlorophenoxyacetic acid on nTiN doped Pd/Ni foam electrode, Chem. Eng. J. 281 (2015) 183–191, https://doi.org/10.1016/j.cej.2015.06.113.
[46] Z. He, Q. Jian, J. Tang, T. Xu, J. Xu, Z. Yu, J. Chen, S. Song, Improvement of electrochemical reductive dechlorination of 2,4-dichlorophenoxyacetic acid using palladium catalysts prepared by a pulsed electrodeposition method, Electrochim. Acta 222 (2016) 488–498, https://doi.org/10.1016/j.electacta.2016.11.001.
[47] W. Yu, H. Jiang, J. Fang, S. Song, Designing an electron-deficient $Pd/NiCo_2O_4$ bifunctional electrocatalyst with an enhanced hydrodechlorination activity to reduce the consumption of Pd, Environ. Sci. Technol. 55 (14) (2021) 10087–10096, https://doi.org/10.1021/acs.est.1c01922.
[48] Q. Liu, Y. Shen, S. Song, Z. He, Enhanced electrocatalytic hydrodechlorination of 2,4-dichlorophenoxyacetic acid by a $Pd\text{-}Co_3O_4$/Ni foam electrode, RSC Adv. 9 (21) (2019) 12124–12133, https://doi.org/10.1039/c9ra01843c.
[49] L. Liu, Y. Chen, S. Li, W. Yu, X. Zhang, H. Wang, J. Ren, Z. Bian, Enhanced electrocatalytic cathodic degradation of 2,4-dichlorophenoxyacetic acid based on a synergistic effect obtained from Co single atoms and Cu nanoclusters, Appl. Catal. B Environ. 332 (2023) 122748, https://doi.org/10.1016/j.apcatb.2023.122748.
[50] Y. Cai, Y.H. Luo, X. Long, M.A. Roldan, S. Yang, C. Zhou, D. Zhou, B.E. Rittmann, Reductive dehalogenation of herbicides catalyzed by Pd^0NPs in a H_2-based membrane catalyst-film reactor, Environ. Sci. Technol. 56 (24) (2022) 18030–18040, https://doi.org/10.1021/acs.est.2c07317.
[51] X. Shu, Q. Yang, F. Yao, Y. Zhong, W. Ren, F. Chen, J. Sun, Y. Ma, Z. Fu, D. Wang, X. Li, Electrocatalytic hydrodechlorination of 4-chlorophenol on Pd supported multi-walled carbon nanotubes particle electrodes, Chem. Eng. J. 358 (2019) 903–911, https://doi.org/10.1016/j.cej.2018.10.095.
[52] H. Zeng, G. Zhang, Q. Ji, H. Liu, X. Hua, H. Xia, M. Sillanpaa, J. Qu, pH-Independent production of hydroxyl radical from atomic H*-mediated electrocatalytic H_2O_2 reduction: a green Fenton process without byproducts, Environ. Sci. Technol. 54 (22) (2020) 14725–14731, https://doi.org/10.1021/acs.est.0c04694.
[53] J. Zhou, M. Wen, R. Huang, Q. Wu, Y. Luo, Y. Tian, G. Wei, Y. Fu, Regulating active hydrogen adsorbed on grain boundary defects of nano-nickel for boosting ammonia electrosynthesis from nitrate, Energy Environ. Sci. 16 (6) (2023) 2611–2620, https://doi.org/10.1039/d2ee04095f.
[54] R. Zhang, J. Li, B. Wang, L. Ling, Fundamental studies about the interaction of water with perfect, oxygen-vacancy and pre-covered oxygen $Cu_2O(111)$ surfaces: thermochemistry, barrier, product, Appl. Surf. Sci. 279 (2013) 260–271, https://doi.org/10.1016/j.apsusc.2013.04.078.
[55] L.Y. Liu, M.H. Cui, S.M. Niu, X.D. Zhang, X.H. Li, W.L. Wang, H. Liu, G.S. Liu, A. J. Wang, Phosphorus-coordinated Pd@MXene electrocatalyst for efficient electrocatalytic hydrodechlorination of diclofenac, ACS EST Eng. (2024), https://doi.org/10.1021/acsestengg.3c00493.